Minimal Wide-Range Resistive Sensor-to-Microcontroller Interface for Versatile IoT Nodes

Alessandro Depari, *Member, IEEE*, Paolo Bellagente, *Member, IEEE*, Paolo Ferrari, *Member, IEEE*, Alessandra Flammini, *Senior Member, IEEE*, Marco Pasetti, *Member, IEEE*, Stefano Rinaldi, *Member, IEEE*, and Emiliano Sisinni, *Member, IEEE*

***Abstract*— Sensor interface is a term including all the circuits adopted for providing measurement readouts from sensor signals. Starting from early 2000s, a plethora of solutions, generally addressed as direct sensor-to-microcontroller interfaces, has been proposed. This concept is particularly intriguing given the widespread adoption of smart devices following the introduction of the Internet of Things (IoT) paradigm. However, the use of those strategies is often limited by the reduced input dynamic range they offer. In this article, authors propose a novel universal interface for resistive sensors, able to provide an overall measurement range larger than 100 dB, combining consecutive subranges leveraging on volt-amperometric and integral measurement approaches. The procedure for determining subranges is detailed; error analysis for estimating the impact of (active components) nonidealities is furnished as well. Moreover, to evaluate feasibility and obtainable performance, a proof-of-concept prototype has been implemented. In particular, a relative error of 1.31% results for fixed resistor measurements ranging from less than 1 kΩ to more than 100 MΩ. The capability to track slowly changing measurand (a common scenario in many IoT applications) has been also verified, given a maximum measurement time of about 0.6 s.**

***Index Terms*— Gas sensor, Internet of Things (IoT), light-dependent resistor (LDR), microcontroller (μC), resistive sensor interface, smart sensor.**

I. Introduction and Motivation

SENSORS are one of the basing building blocks of the so-called smart "things" we find in any Internet of Things (IoT) or Ambient Intelligence (AmI) applications. These paradigms, which are changing the way we live our lives, leverage on intelligent devices that are aware of the surrounding environment and operate accordingly. Generally speaking, first physical quantities of interest are sensed, then embedded computation capabilities allow to extract/process refined information that is finally transferred, by means of integrated communication interfaces, toward cloud infrastructures. Such an approach limits the complexity (and, as a consequence, cost and power consumption) of things, exploiting the "infinite" resources of cloud computing. The wider and wider adoption of IoT and AmI is turning into an increasing demand for versatile and flexible solutions that are able to manage different sensor types, often arranged into an array configuration. Among them, resistive sensors are good candidates for many different applications, since devices able to transduce light intensity, force and pressure, temperature, and humidity are available. Moreover, once properly functionalized, they can detect and analyze chemical compounds (as in electronic noses).

However, despite the actual applications dictate requirements, such as the sampling rate and the resolution, some common needs can be highlighted, for instance; long lifetime, wide dynamic range, and low cost. In addition, IoT nodes have usually limited power resources, so that consumption minimization is required as well; as a consequence, even if sampling rate can be very slow, attention has to be paid to reduce active measurement time. As a matter of fact, several purposely designed, integrated solutions have been presented trying to satisfy these needs.

Some researchers pursued a different approach. In literature, it has been already highlighted that, since a microcontroller (μC) is present in an IoT smart thing, a direct sensor-to-μC interface could be a good tradeoff between complexity and performance. However, as better detailed in Section II, these solutions generally rely on charging a reference capacitor by a current depending on the sensor output and then measuring the discharge time. The time interval is generally measured by the free running counter embedded in the μC time processing unit (TPU), captured by a hardware comparator signaling that the capacitor voltage has crossed a fixed threshold value.

In the current work, authors exploit an analog to digital converter (ADC, generally also available in μCs) to evaluate the voltage drop across a reference capacitor in a fixed time

Manuscript received 25 January 2022; revised 22 April 2022; accepted 2 May 2022. Date of publication 13 May 2022; date of current version 1 June 2022. This work was supported in part by the Project SWaRM-Net through the Ministero dell'istruzione, dell'università e della ricerca (MIUR) 2012 Smart Cities and Communities Grant under Grant SCN_00198. The Associate Editor coordinating the review process was Dr. Fabricio Guimaraes Baptista. *(Corresponding author: Alessandro Depari.)*

The authors are with the Department of Information Engineering, University of Brescia, 25123 Brescia, Italy (e-mail: alessandro.depari@unibs.it; paolo.bellagente@unibs.it; paolo.ferrari@unibs.it; alessandra.flammini@unibs.it; marco.pasetti@unibs.it; stefano.rinaldi@unibs.it; emiliano.sisinni@unibs.it).

Digital Object Identifier 10.1109/TIM.2022.3175045

interval. Since this voltage is the integral of the sensor-dependent capacitor current, this method is referred to as the "integral" approach. In addition, multiple ADC readings can be carried out at well-known time instants, allowing to easily manage different sensor ranges. Furthermore, using the same interface, it is possible to implement the so-called "volt-amperometric" method as well; in this case, a fixed voltage is applied across the sensor and the resulting sensor-dependent current, flowing in a reference resistor, is measured with a single ADC readout, permitting a shorter measurement interval.

The proposed interface requires a very small number of external components: few passive elements, an analog switch, and a single operational amplifier (OA). The main original contributions of this work are:

1) Identification of the need for versatile resistive sensor interface for addressing IoT application requirements.
2) Design of a novel sensor-to-μC interface for resistive sensors.
3) Analysis of possible error sources due to device nonidealities.
4) Implementation of prototype for a real-world experimental testbed.
5) Execution of an experimental campaign for performance characterization using sensor emulations.

The article is arranged as follows: a brief overview of related works is provided in Section II; in Section III, the proposed interface is discussed, whereas Section IV analyses the error sources and their impact; Section V is reserved for experimental results; finally, in Section VI, conclusions are drawn.

II. Related Works

It is well-known that, no matter the actual application scenario, the sensing layer is one of the fundamental pillars in any IoT abstraction model, complemented by an embedded processor performing preliminary, local, signal processing. In particular, the core measurement application is often based on the acquisition of different physical quantities [1], which in turn require different signal conditioning chains providing numerical readouts.

Resistive sensors are widely diffused, thanks to the advantages they offer, as fast response, AC (permitting to reuse interfaces for capacitive sensors [2]) or DC excitation [3], and possibility of being realized through additive manufacturing [4]. However, when embedded into an IoT device, low-power consumption is mandatory, due to limited power source availability. For this reason, in the recent past, a plethora of works appeared in literature provides energy efficient sensor readout circuits. For instance, in [5], a ratiometric architecture is discussed for improving rejection with respect to temperature and supply voltage variation, offering submicrowatt power consumption; however, the range is limited to 30 kΩ. In many applications, a wide measurement range is a main concern [6]–[11]. A sensor range, up to 10 MΩ, has been obtained in [12], leveraging on a logarithmic subrange detector for resistance-to-voltage signal compression.

In contrast, it must be also highlighted that the versatility of the sensor interface is another key requirement; e.g., capacitive sensors also play an important role in the IoT ecosystems. Accordingly, researchers started looking for multisensor interfaces [13]. In [14], an all-dynamic approach is suggested for a multisensor interface, able to tradeoff the performance with the consumption depending on the application needs; however, also in this case, the range is limited to 30 kΩ. In [15], resistance up to 5.9 kΩ and capacitance up to 550 pF are measured exploiting a switched capacitor-based architecture.

The main task of all the previous works is the development of "brand new" interfaces providing digital readouts of the quantity of interest. However, because most IoT-applications are built around μCs, as previously stated, a different approach is to rely on embedded peripherals, to reduce the number of external components. The idea was initially suggested in early 2000s [16]. Since then, many works have been published, proposing improvements in terms of reduced power consumption, acquisition time, and capability to manage different sensor types. Latest works are reviewed hereinafter. In [17], the low-power consumption challenge is addressed, proposing a design methodology for satisfying desired uncertainty and measurement range (when limited dynamic range is tolerated); a low-noise voltage regulator is considered for enhancing power supply rejection. In [18], a three-cycle procedure is implemented for taking into account lead resistances for sensor with limited dynamic, using external switches for implementing different charge/discharge paths; the work has been improved by Anandanatarajan *et al.* [19], where an external resistance-to-time converter is considered, but measurement time is reduced. In [20], capacitively coupled resistive sensors are addressed, providing 5-ms measurement time and a range up to 800 kΩ. In all the aforementioned works, the measurement principle is the resistance-to-time conversion (i.e., the integral measurement strategy); the readout is obtained evaluating, by means of the TPU embedded in the μC, the time interval needed by a reference capacitor (charged/discharger by a sensor-dependent current) to cross a fixed threshold. As a consequence, once the circuit is designed for a certain measurement range, and it is not possible to modify the measurement time (which depends on the measurand value).

In [21], the direct approach is considered as well. However, instead of waiting for the crossing of a fixed comparator threshold, the readout of the μC internal ADC is acquired at a fixed time interval. This approach offers several advantages: to allow for fast volt-amperometric strategy when the range is limited, to use the integral strategy for wider range, and to dynamically modify the range, without using multiple circuit paths that need for complex (matched) switch networks and/or connections to different μC pins. This work largely extends the embryonic idea of [21]; in particular, the aforementioned technique has been further improved, expanding the range of the integral approach by adding new sample time instants. Despite the circuit complexity remains the same, now the overall input range can be tuned according to the application of interest, with the only main drawback of an increment of the measuring time with increasing input range.

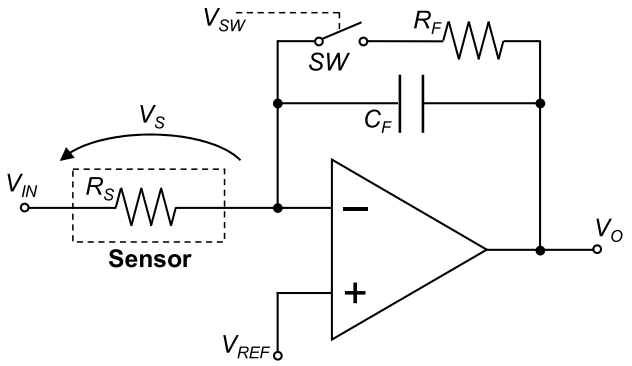

Fig. 1. Block scheme of the proposed sensor interface.

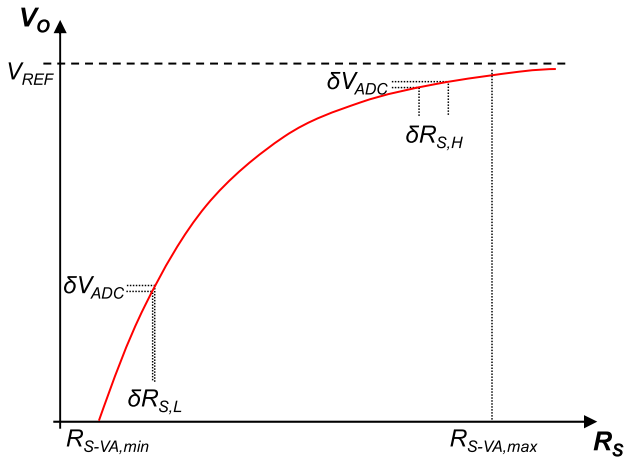

Fig. 2. Circuit output voltage V_O versus sensor resistance R_S in the volt-amperometric mode.

III. Proposed Interface

In some application scenarios, the resistive sensor dynamic range can be quite large. Light-dependent resistors (LDRs) are example of low-cost and widely used devices, exhibiting a resistive range in the order of 40 dB or more [22]. Even worse if the considered application needs to manage a family of sensors with similar characteristics, but different baseline. Some commercial LDR devices such as NORPS-12 from Advanced Photonix and 02-LDR from NTE Electronics have similar dynamic range, but the aggregate dynamic range is about 88 dB. Some experimental gas sensors also exhibit a very wide dynamic range, often exceeding 80 dB [23]. In order to satisfy those requirements, the proposed sensor interface, shown in Fig. 1, trades off the dynamic range against the measurement time. The circuit excites the sensor with a constant voltage V_S and provides an output signal V_O that can be acquired through the ADC of a μC. Since μCs are usually powered by a unipolar positive voltage 0–V_{CC}, the same power supply is used for the sensor frontend.

Two operating modes are defined, according to the status of the switch *SW*: "volt-amperometric" (*SW* closed), and "integral" (*SW* open). Since V_{IN} and V_{REF} are positive DC voltages, the sensor excitation voltage $V_S = V_{IN} - V_{REF}$ is a positive DC voltage as well.

A. Volt-Amperometric Mode

In the volt-amperometric mode (*VA* in the following), the circuit behaves as an inverting amplifier; since the time constant $R_F \cdot C_F$ can be designed to be orders of magnitude less than the sensor R_S variations, the effect of C_F can be neglected. The output voltage V_O as a function of the sensor resistance R_S can be computed as in (1). Conversely, if V_O is acquired (e.g., by an ADC), an estimation $\langle R_S \rangle$ of R_S can be obtained by using the relation in (2)

$$V_O = V_{REF} - \frac{R_F}{R_S}(V_{IN} - V_{REF}) \tag{1}$$

$$\langle R_S \rangle = \frac{V_{IN} - V_{REF}}{V_{REF} - V_O} R_F. \tag{2}$$

In the *VA* mode, lower ($R_{S-VA,min}$) and upper ($R_{S-VA,max}$) limits to the R_S exist. In particular, as visible in (1), $R_{S-VA,min}$ depends on the minimum value that V_O can reach; since the interface is powered with the unipolar power supply 0–V_{CC}, the minimum V_O value is zero, thus yielding to the following equation:

$$R_{S-VA,min} = \left(\frac{V_{IN}}{V_{REF}} - 1\right) R_F. \tag{3}$$

As can be deduced from (1) and reported in Fig. 2, there is a V_O compression effect as R_S increases. Since V_O is acquired through an ADC, the same quantization interval δV_{ADC} corresponds to a resistance deviation $\delta R_{S,L}$ when R_S is in the lower part of the range and a resistance deviation $\delta R_{S,H}$ when R_S is in the higher part of the range, with $\delta R_{S,H} > \delta R_{S,L}$.

Hence, the R_S range upper bound is given by the ADC resolution n and by the maximum tolerated error $\varepsilon_{rel,max}$ (being $\varepsilon_{rel} = |\langle R_S \rangle - R_S|/R_S$) due to ADC quantization. Moreover, in detail, considering an ADC with 0–V_{REF} input range and $\pm 1/2$ LSb of quantization error, the upper bound of the *VA* mode $R_{S-VA,max}$ can be computed by the following equation:

$$R_{S-VA,max} = 2 \cdot 2^n \frac{V_{IN} - V_{REF}}{V_{REF}} R_F \cdot \varepsilon_{rel,max}. \tag{4}$$

The dynamic range DR_{VA} of the *VA* mode can be computed by (5), which is obtained combining (3) and (4). As an example, when $n = 10$ (the typical resolution of ADCs embedded in low-cost μCs) and $\varepsilon_{rel,max} = 1\%$, $DR_{VA} \approx 20$ (26 dB)

$$DR_{VA} = \frac{R_{S-VA,max}}{R_{S-VA,min}} = 2 \cdot 2^n \cdot \varepsilon_{rel,max}. \tag{5}$$

B. Integral Mode

When the switch *SW* of Fig. 1 is open, the circuit behaves as an integrator, thus justifying the name integral mode (*I* in the following). Without loss of generality, for the following explanation, it is considered that the switch *SW* is opened at $t = 0$, supposing that the previous transient is expired; the corresponding initial output value $V_O(0)$ depends on R_S and can be computed by (1). Under the hypothesis that R_S is (quasi) stationary, the output voltage $V_O(t)$ can be obtained

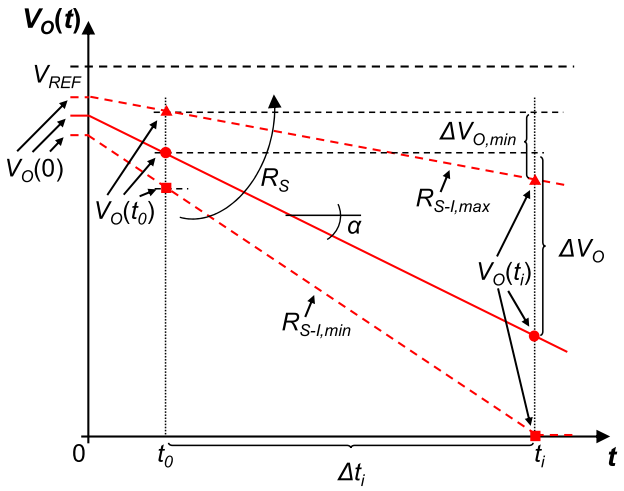

Fig. 3. Circuit output voltage $V_O(t)$ in the integral mode with upper and lower bounds of sensor resistance R_S.

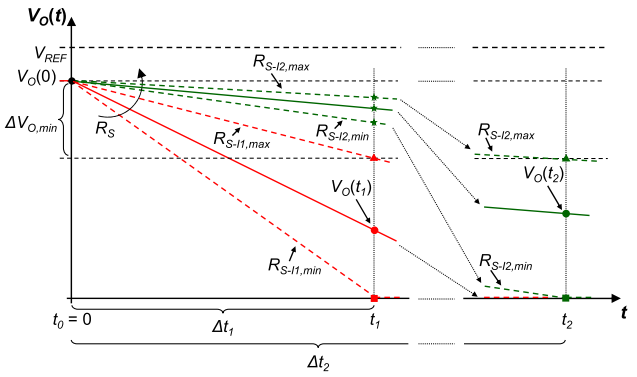

Fig. 4. Circuit output voltage $V_O(t)$ in the integral mode with two sample time instants t_1 and t_2.

by (6); $V_O(t)$ is a falling ramp starting from $V_O(0)$, and the slope α of which depends on the R_S value, as shown in Fig. 3

$$V_O(t) = V_O(0) + \alpha \cdot t = V_O(0) - \frac{V_{IN} - V_{REF}}{R_S C_F} t. \tag{6}$$

Two samples $V_O(t_0)$ and $V_O(t_i)$ of $V_O(t)$ are taken at $t = t_0$ and $t = t_i$, with $t_0 < t_i$. Under the hypothesis that $V_O(t_i)$ is not saturated to zero, an estimation of the sensor resistance R_S can be obtained exploiting (6), as described in the following equation:

$$\langle R_S \rangle = \frac{V_{IN} - V_{REF}}{\Delta V_O C_F} \Delta t_i \quad \text{with} \quad \begin{matrix} \Delta V_O = V_O(t_0) - V_O(t_i) \\ \Delta t_i = t_i - t_0. \end{matrix} \tag{7}$$

As for the *VA* mode, *I* mode lower ($R_{S-I,min}$) and upper ($R_{S-I,max}$) limits to the R_S exist. As shown in Fig. 3, $R_{S-I,min}$ is the resistance value at which $V_O(t)$ saturates at zero exactly in $t = t_i$; R_S lower than $R_{S-I,min}$ would yield to $V_O(t)$ saturation before reaching $t = t_i$, thus invalidating (6) and (7). The $R_{S-I,min}$ value can be obtained by inverting (6), setting $t = t_i$, $V_O(t_i) = 0$, and computing $V_O(0)$ as in (1), thus obtaining the following equation:

$$R_{S-I,min} = \frac{V_{IN} - V_{REF}}{V_{REF}} \left(R_F + \frac{t_i}{C_F} \right). \tag{8}$$

Similar to the *VA* mode, the upper bound $R_{S-I,max}$ of the *I* mode depends on the ADC resolution n and the maximum tolerated error $\varepsilon_{rel,max}$ on the estimation of R_S due to ADC quantization. In fact, as reported in (7) and shown in Fig. 3, given Δt_i and increasing values of R_S, ΔV_O becomes smaller (reduced V_O slope) and hence more affected by the ADC quantization error, A lower limit $\Delta V_{O,min}$ thus exists. By considering an ADC with the same characteristics as before and that ΔV_O is the difference of two V_O samples (quantization error is doubled), the upper bound $R_{S-I,max}$ is given by the following equation:

$$R_{S-I,max} = 2^n \frac{V_{IN} - V_{REF}}{V_{REF}} \frac{\Delta t_i}{C_F} \varepsilon_{rel,max}. \tag{9}$$

The combination of (8) and (9) yields to the expression in (10), which indicates the dynamic range DR_I of the *I* mode. As an example, when $n = 10$ and $\varepsilon_{rel,max} = 1\%$, considering the best case, i.e., $R_F = 0$ and $t_0 = 0$, then $DR_I \approx 10$ (20 dB)

$$DR_I = \frac{R_{S-I,max}}{R_{S-I,min}} = 2^n \frac{\Delta t_i}{t_i + R_F C_F} \varepsilon_{rel,max}. \tag{10}$$

Different range bounds can be obtained by properly choosing the Δt_i value, as illustrated in Fig. 4, where two sample time instants t_i with $i = 1$, 2 and $t_2 > t_1$, are considered. For the sake of graphical simplicity, the ramp starting point $V_O(0)$ has been represented as a constant value for all the involved R_S values, provided that the actual values of $V_O(0)$ can be always obtained by (1). Moreover, without losing generality, the sample time instant t_0 has been set to zero, thus $V_O(t_0) = V_O(0)$.

The minimum and maximum R_S values that can be estimated with the sample at t_1, computed by means of (8) and (9), with $i = 1$, are indicated in Fig. 4 as $R_{S-I1,min}$ and $R_{S-I1,max}$, respectively. Similarly, the $R_{S-I2,min}$ and $R_{S-I2,max}$ values shown in Fig. 4 can be obtained by means of (8) and (9), with $i = 2$. It should be noticed that, since $t_2 > t_1$, $R_{S-I2,min} > R_{S-I1,min}$ and $R_{S-I2,max} > R_{S-I1,max}$; moreover, the expression in (10), with the previously-considered best case, demonstrates that the dynamic range of the R_S estimation with the sample at t_1 and with the sample at t_2 is the same.

C. Proposed Combined Approach

According to (5) and (10), given the tolerated error $\varepsilon_{rel,max}$, both the aforementioned modes need for increased ADC resolution n to extend the dynamic range. This is frequently not possible due to low cost constraints; in such cases, multiple-scale architectures with different feedback resistors R_F or capacitors C_F, selectable by a network switch, are employed. However, such solutions are heavily affected by switch nonidealities and need for an accurate matching of feedback resistor/capacitor values.

The proposed solution offers a first dynamic range expansion by configuring the frontend of Fig. 1 to merge the ranges of the *VA* an *I* modes; in particular, the *VA* mode is used at the lower part of the overall range ($R_{S,min} - R_{S,max}$) and

the I mode in the upper one. In other words, the circuit parameters can be tuned in order to obtain $R_{S,min} = R_{S-VA,min}$, $R_{S-VA,max} = R_{S-I,min}$, and $R_{S-I,max} = R_{S,max}$. Such idea has been introduced in [21].

The second method proposed for increasing the dynamic range makes a smart use of the capability of sampling $V_O(t)$ at different sample times, when operating in the integral mode. In fact, by properly configuring the circuit parameters, it is possible to set $R_{S-I2,min} = R_{S-I1,max}$; in other words, t_1 and t_2 define two integral subranges, which are merged together to form a doubled integral range spanning from $R_{S-I1,min}$ to $R_{S-I2,max}$. Interesting to note, more integral subranges can be added via additional sampling points t_i, with $i > 2$, leading to a further expansion of the overall R_S range; the obvious limitation is the increasing sampling time, which could become too large for a specific application.

The proposed solution takes advantage of both the aforementioned range expansion methods; in the following, the steps to be followed for the circuit parameter configuration are detailed.

1) First, being $R_{S,min}$ the desired minimum value of R_S, the R_F value is derived by inverting (3), considering $R_{S-VA,min} = R_{S,min}$.
2) The upper bound of the volt-amperometric mode ($R_{S-VA,max}$) is computed with (4) and set equal to the lower bound of the first integral subrange ($R_{S-I1,min}$).
3) Once the sample time instants t_0 and t_1 have been chosen, according to the obtainable performance in time interval evaluation by the TPU, the C_F value is reckoned by inverting (8), considering $R_{S-I,min} = R_{S-I1,min} = R_{S-VA,max}$ and $i = 1$.
4) The upper bound of the first integral subrange ($R_{S-I1,max}$) is computed with (9), with $i = 1$, and set equal to the lower bound of the second integral subrange ($R_{S-I2,min}$).
5) The sample time t_2 is reckoned by inverting (8), where $R_{S-I,min} = R_{S-I2,min} = R_{S-I1,max}$. Interesting to note, the t_2 value is equal to t_1 multiplied by the dynamic range of the first integral subrange.
6) The upper bound of the second integral subrange ($R_{S-I2,max}$) is computed with (9), with $i = 2$.
7) If more integral subranges have to be added, the procedure is iterated by designing the next sample times t_i, with $i > 2$.
8) The upper bound of the last added subrange sets the upper limit $R_{S,max}$ of the overall R_S range (e.g., $R_{S,max} = R_{S-I2,max}$ with two integral subranges).

For instance, when the volt-amperometric mode is combined with two adjacent integral subranges, the proposed approach allows to obtain a dynamic range $DR \approx 2000$ (66 dB), if a 10-bit resolution ADC and $\varepsilon_{rel,max} = 1\%$ are considered, with $t_2 \approx 10t_1$. Two additional integral subranges will allow to obtain $DR \approx 200\,000$ (106 dB), with $t_4 \approx 1000t_1$.

IV. Error Analysis

The focus of this section is to evaluate the performance of the proposed interface in terms of resistance estimation considering error sources due to real-world components, reducing as much as possible the variability of the measurand (which depends on the target application). Accordingly, only static nonidealities of the analog frontend connected to the μC are considered.

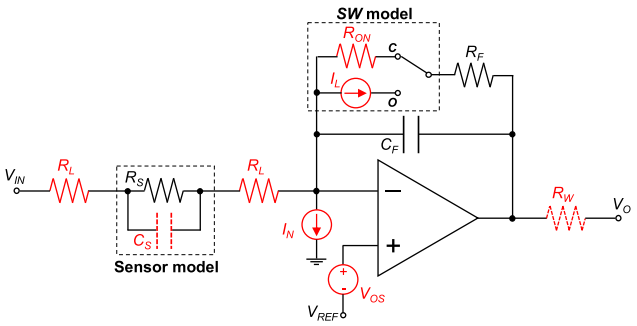

Fig. 5. Proposed frontend with the considered circuit nonidealities.

For the sake of completeness, the resulting static errors in the sensor resistance estimation (supposing all transients are expired) are detailed in the following. Errors imputable to other external affecting quantities, as the deviation from the expected value of the sensor excitation voltage, in the sampling instants, and in the converter readouts are not analytically assessed, but included in the experimental evaluation (see Section V).

The schematic in Fig. 5 shows the frontend circuit and the error sources (highlighted in red). The lead resistances R_L, the OA voltage offset V_{OS}, and the bias current I_N are taken into account. The wire resistance R_W is ignored because of the μC high input impedance; in contrast, being the sensor excited with DC voltage, the parasitic capacitance C_S has no effect. Regarding the former, the frontend is close to the μC input, so that $R_W \ll R_{in,\mu C}$, being $R_{in,\mu C}$ the μC input resistance. Regarding the latter, the voltage drop across C_S is constant; moreover, the capacitance C_F has to be considered only for the integral mode for the same reason. As regards the switch SW, when the volt-amperometric method is employed, it can be modeled by the ON-resistance R_{ON} (C position of SW model in Fig. 5); in case of integral mode, it is modeled as a current generator whose value is the leakage I_L (O position of SW model in Fig. 5). Effects related to the switch SW charge injection and clock feedthrough lead to a V_O voltage step during the switch opening, thus altering the ramp starting value $V_O(0)$; indeed, this can reduce the actual $V_O(t)$ range, but the ramp slope α (see Fig. 3) is not affected. Since a two-point estimation of ΔV_O is carried out in the integral mode and the initial sample is acquired in $t_0 \neq 0$, the switch SW charge injection and clock feedthrough effects can be ignored for the sake of error analysis. For the same reason, delay in the switching activity can also be ignored. Interesting to note, in this way, the aperture time in the V_O conversion equally impacts sampling instants t_0 and $t_{i\neq 0}$, so that Δt_i estimations are only affected by the (much smaller) jitter.

The absolute error has been estimated as $\varepsilon_X = |\langle R_{S,X}\rangle - R_S|$, where $X = VA$ for the volt-amperometric mode or $X = I$ for the integral one, respectively. Therefore, the relative error can be computed as $\varepsilon_{rel,X} = \varepsilon_X / R_S = |\langle R_{S,X}\rangle - R_S| / R_S$.

A. Lead Resistance

Effects of (long) sensor leads can be summed up in two equivalent resistors in series with the sensor; supposing equal lengths, they both have R_L resistance. Consequently, errors are

$$\begin{aligned}\varepsilon_{VA}(R_L) &= \varepsilon_I(R_L) = 2R_L \\ \varepsilon_{rel,VA}(R_L) &= \varepsilon_{rel,I}(R_L) = \frac{2R_L}{R_S}.\end{aligned} \tag{11}$$

However, in most of target applications, where the sensor is part of an IoT smart thing, leads are short and R_L is negligible.

B. OA Input Voltage Offset

The OA offset voltage V_{OS} changes the voltage drop across the sensor and consequently the current flowing in the OA feedback network. In particular, after few manipulations, the following relations can be obtained:

$$\begin{aligned}\varepsilon_{VA}(V_{OS}) &= R_S \frac{V_{OS}(R_S + R_F)}{R_F(V_{IN} - V_{REF} - V_{OS}) - R_S V_{OS}} \\ &= R_S \varepsilon_{rel,VA}(V_{OS})\end{aligned} \tag{12}$$

$$\varepsilon_I(V_{OS}) = R_S \frac{V_{OS}}{V_{IN} - V_{REF} - V_{OS}} = R_S \varepsilon_{rel,I}(V_{OS}). \tag{13}$$

C. OA Bias Current

The OA bias current flows in the feedback network; as a consequence

$$\begin{aligned}\varepsilon_{VA}(I_N) &= \varepsilon_I(I_N) = R_S \frac{I_N R_S}{V_{IN} - V_{REF} - I_N R_S} \\ &= R_S \varepsilon_{rel,VA}(I_N) = R_S \varepsilon_{rel,I}(I_N).\end{aligned} \tag{14}$$

D. Switch ON-Resistance and Leakage Current

The switch ON-resistance has to be considered when the volt-amperometric mode is adopted; in this case, an additional R_{ON} is in series with the feedback resistor, resulting in

$$\varepsilon_{VA}(R_{ON}) = R_S \frac{R_{ON}}{R_F + R_{ON}} = R_S \varepsilon_{rel,VA}(R_{ON}). \tag{15}$$

As regards the leakage current, considered in the integral mode only, it behaves the same way the OA bias current, therefore

$$\varepsilon_I(I_L) = R_S \frac{I_L R_S}{V_{IN} - V_{REF} - I_L R_S} = R_S \varepsilon_{rel,I}(I_L). \tag{16}$$

As a concluding remark, it can be highlighted that, as expected, errors can be minimized applying as large as possible $V_S = V_{IN} - V_{REF}$ voltage across the sensor. In Section V, numerical values considering a proof of concept prototype with real-world components will be provided.

V. Experimental Characterization

To evaluate the performance of the proposed architecture, a proof-of-concept prototype of the sensor interface in Fig. 1 has been designed around an OPA350 OA from Texas Instruments ($V_{OS} \approx 150$ μV, $I_N \approx 1$ pA), a MAX4641 analog switch from Maxim Integrated ($R_{ON} \approx 2.5$ Ω, $I_L \approx 10$ pA), and discrete resistors/capacitors. The interface circuit is managed by the ATMega32u4 μC hosted in an Adafruit Feather 32u4 Bluefruit LE board. The USB bus furnishes the circuit power supply $V_{CC} = V_{IN} = 5$ V; a voltage regulator (on the same board) provides $V_{REF} = 3.3$ V, which is also used as the ADC reference voltage. According to the specific application, such voltages should be chosen to properly excite the sensor with $V_S = V_{IN} - V_{REF}$ and considering that: 1) V_{REF} must be within the supply rails of the interface; 2) $V_{IN} > V_{REF}$; and 3) V_{IN} must have low-impedance output. In general, the larger V_S, the larger the sensitivity. In this work, the choice of using the available power supplies as V_{IN} and V_{REF} is merely for the sake of circuit simplicity.

TABLE I

Lower and Upper R_S Bounds in Each Range and Sample Time Intervals for Integral Subranges

	VA	I_1	I_2	I_3	I_4
$R_{S,min}$	950 Ω	16.0 kΩ	130 kΩ	1.15 MΩ	10.0 MΩ
$R_{S,max}$	19.0 kΩ	150 kΩ	1.30 MΩ	11.5 MΩ	101 MΩ
t_i $(i \geq 1)$	N.A.	928.0 µs	7.968 ms	70.94 ms	617.3 ms

The ADC embedded in the μC has a nominal resolution $n = 10$ bits. The TPU of the μC works with a clock frequency of 8 MHz, prescaled by a factor 256; thus, the time resolution for the generation of the sample time instants is 32 μs. In order to reduce jitter in the sampling instants, the ADC is triggered by TPU output compare feature.

Commercial (gas) sensors like the TGS2602 from Figaro as well as experimental sensors as in [24] have been considered as a reference for the configuration of the input resistive range. Such devices show a resistive behavior in the typical range of 1 kΩ–100 MΩ, which will be considered as the desired input range of the proposed (universal) interface. Having in mind a typical IoT-like application scenario, a slowly changing quantity of interest is supposed, affording a maximum measurement time of 1 s. Finally, a target tolerated error $\varepsilon_{rel,max} = 1\%$ is set.

The integral mode has been divided into four subranges, named I_i with $i = 1, \ldots, 4$. The first two sample instants have been set to $t_0 = 32$ μs and $t_1 = 928$ μs, respectively, whereas other sample instants are dictated by the range design procedure in Section III-C. In order to minimize effects due to discrete component nonidealities and tolerances, a reduced voltage V_O range has been considered (20 mV–3.3 V), limiting saturation problems; additionally, a partial overlap of the ranges has been set, i.e., $R_{S-VA,max} > R_{S-I1,min}$ and $R_{S-Ii,max} > R_{S-Ii+1,min}$ for $i \geq 1$. Thus, the aggregate sensor resistance range is smaller than the combination of the single theoretical ones. Following the parameter setting procedure of Section III-C, $R_F = 18$ kΩ and $C_F = 32$ pF have been chosen. The resulting bounds of the volt-amperometric and integral ranges as well as the sampling time t_i for $i \geq 1$ are shown in Table I. It should be noticed that the resulting longest measuring time, i.e., the sample time t_4 related to the subrange I_4, is less than the tolerated maximum measurement time (1 s) for the considered target application.

At first, an evaluation of the expected errors due to the nonidealitites of the employed components has been accomplished, based on the analysis provided in Section IV. Next,

to demonstrate the validity of the proposed approach, two set of experimental tests have been carried out, as detailed in the following. Finally, a comparison with previously considered related works is provided.

A. Evaluation of Expected Errors

According to (11), the lead resistance R_L has the maximum impact on the relative error when the sensor resistance R_S is at its lower value. Since most of the IoT-like applications imply the compactness of the sensor node, $R_L < 1\ \Omega$ can be considered as a meaningful value, yielding to a worst case relative error of about 0.20% (with $R_S = 950\ \Omega$).

According to (12), the OA offset voltage V_{OS} has the maximum impact on the relative error in the volt-amperometric mode when R_S is at its upper value; thus, the worst case relative error is about 0.10% (with $R_S = 19\ \text{k}\Omega$). Conversely, the relation in (13) states that in the integral mode V_{OS} is responsible of a relative error of about 0.01%, independent of the R_S value.

According to (14), the OA bias current I_N impacts on the relative error the same way in the volt-amperometric and integral mode and has its maximum effect with large R_S values; in particular, with $R_S = 100\ \text{M}\Omega$, the relative error due to I_N is about 0.01%.

According to (15), the switch ON-state resistance R_{ON} is responsible, in the volt-amperometric mode only, of a relative error of about 0.14%, independent of the R_S value.

According to (16), the switch leakage current I_L is responsible, in the integral mode only, of a relative error with a maximum effect with large R_S values; in particular, with $R_S = 100\ \text{M}\Omega$, the relative error due to I_L is about 0.06%.

As a final remark, the combined worst case error is on the order of 0.1%, thus one order of magnitude less than the tolerated error due to ADC quantization.

B. System Characterization With Fixed Resistors

The performance of resistance estimation has been evaluated by using reference discrete resistors (1% tolerance) as R_S, spanning in the overall range. The R_S estimation is accomplished using the volt-amperometric mode first (SW closed) and then activating the integral mode (SW open), sampling in all time instants t_i, with $i = 0, \ldots, 4$. The selection of the most accurate method for R_S estimation, according to Table I, has been performed by off-line postprocessing. In case of range overlap, the estimation obtained with the "upper" range is used, since estimation performance is better when R_S in the lower part of each range. For each test resistor value, 100 estimations $\langle R_S \rangle$ have been carried out and the mean value $\langle R_{S,AV} \rangle$ and relative error $\varepsilon_{rel} = |\langle R_{S,AV} \rangle - R_S|/R_S$ computed. For the above computations, a measured value of $V_{IN} = 5.1$ V has been used in place of the nominal 5 V of the USB power supply. It should be noticed that a voltage reference device could be used to generate the V_{IN} voltage. As reported in Table II, the maximum relative error within each range is about 5%, well beyond the target 1% value. This is mainly due to systematic errors imputable to unmodeled

TABLE II
SYSTEM CHARACTERIZATION WITH DISCRETE RESISTORS

	VA	I_1	I_2	I_3	I_4
Max ε_{rel}	2.18%	**4.79%**	4.64%	4.21%	4.02%
Max $\varepsilon_{rel,L}$	0.65%	0.55%	0.97%	**1.31%**	0.43%
Max $\sigma_{rel,L}$	0.56%	0.32%	**0.66%**	0.32%	0.40%

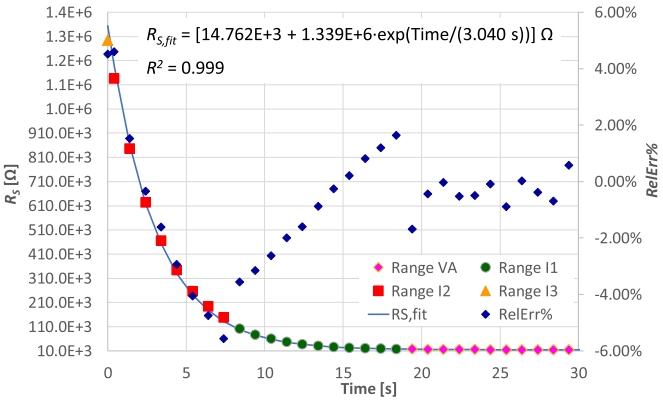

Fig. 6. Acquisition of an emulated time-variable sensor resistance with the proposed system.

circuit nonidealities (e.g., printed circuit board leakage current) and to the tolerance of components.

To minimize the above systematic errors, a calibration procedure, based on linear regression, has been applied to the $\langle R_{S,AV} \rangle$ values of each range, leading to linearized average estimation $\langle R_{S-L,AV} \rangle$; the corresponding maximum values of relative error $\varepsilon_{rel,L} = |\langle R_{S-L,AV} \rangle - R_S|/R_S$ are reported in Table II. The linearization has been able to decrease the maximum relative error to about 1.3% in the overall range, thus validating the proposed approach. The standard deviation σ_L of the linearized estimations has been also computed and the relative value $\sigma_{rel,L} = \sigma_L/R_S$ is shown in the table, with a maximum value less than 0.7% in the aggregated range. It is worth noting that the obtained performance in the resistance estimation is in line with the initial target.

C. Validation With Time-Variable Resistor

In the second test, a time variable resistance $R_S(t)$ has been considered, in order to confirm the capability to dynamically change subranges for tracking physical quantity of interest varying in a wide range. In particular, for the sake of simplicity, the desired $R_S(t)$ has been emulated by applying a variable $V_{IN}(t)$ to a fixed R_S resistor. The actual $V_{IN}(t)$ waveform has been generated by an arbitrary waveform generator (Agilent 33220A, with 14 bit digital to analog converter (DAC) resolution), provided with a purposely designed set of samples. In this way, it has been possible to easily mimic a falling resistance exponential behavior, from about 1.3 MΩ down to about 15 kΩ, with a time constant of 3 s, i.e., the typical resistance variation of gas sensors reacting to target substances [25], [26]. As visible in Fig. 6, the system has been able to correctly track the R_S resistive drop of about two decades, automatically selecting the most appropriate method

TABLE III
COMPARISON WITH RELATED WORKS

	[16]	[17]	[18]	[19]	[20]	This work
Working principle	RT	RT	RT	RT	RT	VA+RT
Dynamic range [dB]	40	3	3	4	24	100
Relative error (max)	0.10%	0.03%	0.06%	0.12%	0.91%	1.31%
Measurement time [ms]	N.D.	< 15	5	3	5	< 620
Complexity	VL	VL	L	M	VL	L
Legenda	*RT (Resistance-to-Time), VA (Volt-Amperometric), N.D. (Not Declared), VL (Very Low), L (Low), M (Medium)*					

and subrange (in this example, from integral subrange I_3 to volt-amperometric range *VA*). The exponential fitting $R_{S,fit}$ of the R_S estimation is reported in the same plot; it shows a very high R^2 value and a time constant compatible with the expected value (3 s), thus demonstrating the validity of the propose approach. In addition, the relative residual error RelErr%, i.e., the deviation of $R_{S,fit}$ from R_S has been computed and reported in Fig. 6. It should be noticed that residual errors are greater than the $\varepsilon_{rel,L}$ values reported in Table II. Deviations from expected behavior are mainly due to the nonstationary emulated sensor value during the measurement process and to some residual calibration errors. Nevertheless, the capability of the proposed system to estimate a real-world sensor-like resistive variation has been fully demonstrated.

It should be noticed that this test does not represent an accurate dynamic characterization of the proposed solution, which is out of the scope of the article. Indeed, considering the volt-amperometric approach, the proposed circuit acts as a first order low-pass filter with time constant $R_F \cdot C_F \approx$ 0.6 ms; sensor variations with (much) larger time constants are expected not to produce significant dynamic errors. Similar considerations can be drawn for the integral approach, where the limit to the dynamic behavior of the sensor is the actual integration time, i.e., the sampling time t_i, according with Table I.

D. Comparison With Related Works

A comparison with related works focused on direct sensor-to-μC interfaces reported in Section II is provided in Table III. As can be seen, the proposed approach represents a good trade-off between dynamic range and performance/measurement time, still offering low complexity, as permitted by the direct interface approach. As a final remark, only the proposed interface is a suitable solution for managing resistive gas and LDR sensors, which are devices exhibiting a very-wide dynamic range (typically larger than 40 dB).

VI. CONCLUSION

The so-called "smart things," i.e., the fundamental building blocks of any IoT applications, are nothing but the next step in the smart sensor evolution. In particular, the "smartness" derives from the embedded μCs they host. For this reason, the use of direct sensor-to-μC interface is particularly attracting, allowing to reduce complexity and cost but preserving performance and flexibility. In this work, a combined volt-amperometric and integral strategy is proposed, for interfacing with resistive sensor. The main advantage of the suggested solution is a wide measurement dynamic range, allowing for the usage in very diverse scenarios involving sensors exploiting different transducing approaches. Starting from a target tolerated error in the order of 1%, the article describes how to define multiple contiguous subranges for managing the overall range, in excess of 100 dB. In such a case, the maximum measurement time is in the order of 0.6 s, suitable for slowly changing quantities of interest, as typically occurs in the considered IoT-like applications. If power-constrained applications need to be addressed, it is possible to devise a low duty-cycle operating mode, i.e., during the integration the μC can be put in a proper low power mode; moreover, the firmware can be designed in order to skip the unnecessary integral measurements, in case a proper estimation has been already obtained. The impact of active components has been analytically modeled. A measurement campaign based on a proof-of-concept prototype has been also carried out, confirming a 1.31% worst case relative error, despite the very simple interface arrangement.

ACKNOWLEDGMENT

The authors would like to thank Alessandro Pancera and Gabriele Racioppa for supporting the experimental setup implementation.

REFERENCES

[1] P. Daponte, F. Lamonaca, F. Picariello, L. D. Vito, G. Mazzilli, and I. Tudosa, "A survey of measurement applications based on IoT," in *Proc. Workshop Metrology Ind. 4.0 IoT*, Apr. 2018, pp. 1–6.
[2] E. Sisinni, A. Depari, A. Flammini, G. Ferri, V. Stornelli, and G. Barile, "Full-analog parasitic capacitance compensation for AC-excited differential sensors," *IEEE Trans. Instrum. Meas.*, vol. 69, no. 8, pp. 5890–5899, Aug. 2020.
[3] R. Pallas-Arany and J. G. Webster, *Sensors and Signal Conditioning*, 2nd ed. New York, NY, USA: Wiley, 2001.
[4] F. Lucklum and G. Dumstorff, "3D printed pressure sensor with screen-printed resistive read-out," in *Proc. IEEE Sensors*, Oct. 2016, pp. 1–3.
[5] H. Xin, P. Baltus, E. Cantatore, and P. Harpe, "A 0.32 nW–1.07 μW all-dynamic versatile resistive sensor interface with system-level ratiometric measurement," *IEEE Trans. Circuits Syst. I, Reg. Papers*, vol. 69, no. 2, pp. 506–517, Feb. 2022, doi: 10.1109/TCSI.2021.3119541.
[6] P. Mantenuto, A. De Marcellis, and G. Ferri, "Uncalibrated analog bridge-based interface for wide-range resistive sensor estimation," *IEEE Sensors J.*, vol. 12, no. 5, pp. 1413–1414, May 2012.
[7] A. D. Marcellis, A. Depari, G. Ferri, A. Flammini, and E. Sisinni, "A CMOS integrated low-voltage low-power time-controlled interface for chemical resistive sensors," *Sens. Actuators B, Chem.*, vol. 179, pp. 313–318, Mar. 2013.
[8] A. Depari, A. Flammini, E. Sisinni, A. De Marcellis, G. Ferri, and P. Mantenuto, "Fast, versatile, and low-cost interface circuit for electrochemical and resistive gas sensor," *IEEE Sensors J.*, vol. 14, no. 2, pp. 315–323, Feb. 2014.
[9] V. Sreenath, K. Semeerali, and B. George, "A resistive sensor readout circuit with intrinsic insensitivity to circuit parameters and its evaluation," *IEEE Trans. Instrum. Meas.*, vol. 66, no. 7, pp. 1719–1727, Jul. 2017.
[10] Z. Hijazi, M. Grassi, D. D. Caviglia, and M. Valle, "153dB dynamic range calibration-less gas sensor interface circuit with quasi-digital output," in *Proc. New Gener. CAS (NGCAS)*, Sep. 2017, pp. 109–112.
[11] F. Ciciotti *et al.*, "A 450-μ a 128-dB dynamic range A/D CMOS interface for MOX gas sensors," *IEEE Sensors J.*, vol. 19, no. 24, pp. 12069–12078, Dec. 2019.

[12] M. Choi, J. Gu, D. Blaauw, and D. Sylvester, "Wide input range 1.7μW 1.2kS/s resistive sensor interface circuit with 1 cycle/sample logarithmic sub-ranging," in *Proc. Symp. VLSI Circuits (VLSI Circuits)*, Jun. 2015, pp. C330–C331.
[13] B. Yousefzadeh, W. Wu, B. Buter, K. Makinwa, and M. Pertijs, "A compact sensor readout circuit with combined temperature, capacitance and voltage sensing functionality," in *Proc. Symp. VLSI Circuits*, Jun. 2017, pp. C78–C79.
[14] H. Xin, M. Andraud, P. Baltus, E. Cantatore, and P. Harpe, "A 0.34–571nW all-dynamic versatile sensor interface for temperature, capacitance, and resistance sensing," in *Proc. ESSCIRC IEEE 45th Eur. Solid State Circuits Conf. (ESSCIRC)*, Sep. 2019, pp. 161–164.
[15] M. M. Moayer, J. Salomaa, and K. A. I. Halonen, "A 0.39–3.56-μW wide-dynamic-range universal multi-sensor interface circuit," *IEEE Sensors J.*, vol. 20, no. 20, pp. 12262–12273, Oct. 2020.
[16] F. Reverter, J. Jordana, M. Gasulla, and R. Pallàs-Areny, "Accuracy and resolution of direct resistive sensor-to-microcontroller interfaces," *Sens. Actuators A, Phys.*, vol. 121, no. 1, pp. 78–87, 2005.
[17] O. López-Lapeña, E. Serrano-Finetti, and O. Casas, "Low-power direct resistive sensor-to-microcontroller interfaces," *IEEE Trans. Instrum. Meas.*, vol. 65, no. 1, pp. 222–230, Jan. 2016.
[18] P. R. Nagarajan, B. George, and V. J. Kumar, "Improved single-element resistive sensor-to-microcontroller interface," *IEEE Trans. Instrum. Meas.*, vol. 66, no. 10, pp. 2736–2744, Oct. 2017.
[19] R. Anandanatarajan, U. Mangalanathan, and U. Gandhi, "Enhanced microcontroller interface of resistive sensors through resistance-to-time converter," *IEEE Trans. Instrum. Meas.*, vol. 69, no. 6, pp. 2698–2706, Jun. 2020.
[20] L. Areekath, B. George, and F. Reverter, "Analysis of a direct microcontroller interface for capacitively coupled resistive sensors," *IEEE Trans. Instrum. Meas.*, vol. 70, pp. 1–10, 2021.
[21] A. Depari *et al.*, "Versatile and low-cost sensor interface for IoT-ready odor monitoring in wastewater management," in *Proc. IEEE Sensors Appl. Symp. (SAS)*, Aug. 2021, pp. 1–6.
[22] D. Hazarika, K. C. Sarma, and P. K. Sarmah, "Microprocessor-based temperature monitoring system using optical fibers," *IEEE Sensors J.*, vol. 9, no. 9, pp. 1025–1028, Sep. 2009.
[23] D. Zappa, "The influence of Nb on the synthesis of WO_3 nanowires and the effects on hydrogen sensing performance," *Sensors*, vol. 19, no. 10, p. 2332, May 2019.
[24] A. Moumen *et al.*, "Robust room-temperature NO_2 sensors from exfoliated 2D few-layered CVD-grown bulk tungsten di-selenide (2H-WSe_2)," *ACS Appl. Mater. Interface*, vol. 13, no. 3, Jan. 2021, pp. 4316–4329.
[25] A. Ponzoni, A. Depari, E. Comini, G. Faglia, A. Flammini, and G. Sberveglieri, "Exploitation of a low-cost electronic system, designed for low-conductance and wide-range measurements, to control metal oxide gas sensors with temperature profile protocols," *Sens. Actuators B, Chem.*, vol. 175, pp. 149–156, Dec. 2012.
[26] C. Schultealbert, T. Baur, A. Schütze, and T. Sauerwald, "Facile quantification and identification techniques for reducing gases over a wide concentration range using a MOS sensor in temperature-cycled operation," *Sensors*, vol. 18, no. 3, p. 744, Mar. 2018.

Alessandro Depari (Member, IEEE) received the M.Sc. degree in electronics engineering and the Ph.D. degree in electronic instrumentation from the University of Brescia, Brescia, Italy, in 2002 and 2006, respectively.

He is currently an Associate Professor with the Department of Information Engineering, University of Brescia. His current research interests include sensor signal conditioning and processing, embedded systems, and design and development of systems for mobile health (mHealth) and Internet of Things (IoT) applications.

Paolo Bellagente (Member, IEEE) is currently an Assistant Professor with the Department of Information Engineering, University of Brescia, Brescia, Italy. His research field is about Internet of Things (IoT) systems for smart city and cognitive buildings applications.

Paolo Ferrari (Member, IEEE) received the M.Sc. degree in electronics engineering and the Ph.D. degree in electronic instrumentation from the University of Brescia, Brescia, Italy, in 1999 and 2003, respectively.

He is currently a Full Professor with the Department of Information Engineering, University of Brescia. His research is about measurement systems for industrial and smart city applications, including performance and security analysis of real-time networks and Internet of Things (IoT) applications; wired and wireless sensor networks; and clock synchronization of distributed systems.

Alessandra Flammini (Senior Member, IEEE) received the M.Sc. degree (Hons.) in physics from the University of Rome, Rome, Italy, in 1985.

After eight years with Ansaldo Industria, Milan, Italy, in 1995, she joined the University of Brescia, Brescia, Italy, where she is currently a Full Professor of electronic measurements. She has authored or coauthored more than 200 international articles. Her current research interests include electronic instrumentation, digital processing of sensor signals, smart sensors, and wired and wireless sensor networks synchronization.

Marco Pasetti (Member, IEEE) is currently an Assistant Professor of electrical energy systems with the Department of Information Engineering, University of Brescia, Brescia, Italy. His main research interests include distributed energy systems, renewable energy sources, energy storage, and supervisory control systems.

Stefano Rinaldi (Member, IEEE) received the M.Sc. degree (Hons.) in electronic engineering and the Ph.D. degree in electronic instrumentation from the University of Brescia, Brescia, Italy, in 2006 and 2010, respectively.

He is currently an Associate Professor with the Department of Information Engineering, University of Brescia. His research interests include industrial real-time ethernet network, Internet of Things, time synchronization, smart grids, renewable energy sources, electric vehicles, and cognitive building.

Emiliano Sisinni (Member, IEEE) received the M.Sc. degree in electronics engineering and the Ph.D. degree in electronic instrumentation from the University of Brescia, Brescia, Italy, in 2000 and 2004, respectively.

He is currently a Full Professor of electronics with the Department of Information Engineering, University of Brescia. His research interests include wireless and wired networking for the Internet of Things (IoT) applications.

Open Access funding provided by 'Università degli Studi di Brescia' within the CRUI CARE Agreement